Geomechanics and Engineering, *Vol. 35, No. 1 (2023) 29-39*
https://doi.org/10.12989/gae.2023.35.1.029

Effects of parallel undercrossing shield tunnels on river embankment: Field monitoring and numerical analysis

Li'ang Chen[1a], Lingwei Lu[1a], Zhiyang Tang[1a], Shixuan Yi[1a], Qingkai Wang[2b] and Zhibo Chen*[3c]

[1]*Guangzhou Metro Design&Research Institute Co.,Ltd., Guangzhou, Guangdong, P.R. China*
[2]*Zhongshan Municipal People's Government Office, Zhongshan, Guangdong, P.R. China*
[3]*Zijin School of Geology and Mining Fuzhou University, Fujian, P.R. China*

(*Received May 31, 2023, Revised August 5, 2023, Accepted August 18, 2023*)

Abstract. As the intensity of urban underground space development increases, more and more tunnels are planned and constructed, and sometimes it is inevitable to encounter situations where tunnels have to underpass the river embankments. Most previous studies involved tunnels passing river embankments perpendicularly or with large intersection angle. In this study, a project case where two EPB shield tunnels with 8.82 m diameter run parallelly underneath a river embankment was reported. The parallel length is 380 m and tunnel were mainly buried in the moderate / slightly weathered clastic rock layer. The field monitoring result was presented and discussed. Three-dimensional back-analysis were then carried out to gain a better understanding the interaction mechanisms between shield tunnel and embankment and further to predict the ultimate settlement of embankment due to twin-tunnel excavation. Parametrical studies considering effect of tunnel face pressure, tail grouting pressure and volume loss were also conducted. The measured embankment settlement after the single tunnel excavation was 4.53 mm ~ 7.43 mm. Neither new crack on the pavement or cavity under the roadbed was observed. It is found that the more degree of weathering of the rock around the tunnel, the greater the embankment settlement and wider the settlement trough. Besides, the latter tunnel excavation might cause larger deformation than the former tunnel excavation if the mobilized plastic zone overlapped. With given geometry and stratigraphic condition in this study, the safety or serviceability of the river embankment would hardly be affected since the ultimate settlement of the embankment after the twin-tunnel excavation is within the allowable limit. Reasonable tunnel face pressure and tail grouting pressure can to some extent suppress the settlement of the embankment. The recommended tunnel face pressure and tail grouting pressure are 300 kPa and 550 kPa in this study, respectively. However, the volume loss plays the crucial role in the tunnel-embankment interaction. Controlling and compensating the tunneling induced volume loss is the most effective measure for river embankment protection. Additionally, reinforcing the embankment with cement mixing pile in advance is an alternative option in case the predicted settlement exceeds allowable limit.

Keywords: field monitoring; river embankment; settlement control; shield tunnel; three-dimensional numerical analysis

1. Introduction

With urbanization accelerating, the demand for underground space development in cities is increasing, especially in cosmopolitan cities, such as pile foundations (Cui *et al.* 2016, Cui *et al.* 2018a, Cui *et al.* 2018b, Cui *et al.* 2020), tunnel and deep basement (Ng *et al.* 2013, Shi *et al.* 2015, Shi *et al.* 2019, Shi *et al.* 2020). Tunnels are widely used in railroads, highways, and urban rail transit industry as one kind of underground infrastructure. In southern China, the water resource is rich. Therefore, it is likely that the tunnel construction process will encounter situations where the line is laid across or even along the river embankment. The disturbance of soil around the tunnel would cause adverse effects on the river embankment, such as settlement, cracks, etc. River embankments are typically located adjacent to urban roads and are an essential part of urban flood control systems. Once the river embankment is damaged, it can seriously affect the safety of the surrounding people and cause significant economic losses. Hence, it is imperative for designers and engineers to have a comprehensive understanding of ground movement caused by tunneling to assess the potential damage to river embankments and take necessary remedial measures.

There have been numerous studies on the tunneling induced ground surface settlement. Gaussian curves are widely used to simulate ground settlement curves, which have been shown to have good agreement with field monitoring and laboratory test results (Peck 1969, O'Reilly and New 1982, New and O'Reilly 1991, Mair *et al.* 1993, Chapman *et al.* 2007). Some scholars study this topic with analytical solution or numerical simulation (Neaupane *et al.* 2006, Park 2004, Chi *et al.* 2001). In addition, some scholars have conducted researches on the impact of earth pressure balance shield tunneling on the surrounding environment (Bai *et al.* 2021, Boonyarak and Ng 2014,

*Corresponding author, Professor
E-mail: 534332303@qq.com
[a]Engineer
[b]Senior Engineer
[c]Professor

ISSN: 2005-307X (Print), 2092-6219 (Online)

Chen *et al.* 2022, Jiang *et al.* 2017, Li and Bai 2022, Nawel and Salah 2015, Ng *et al.* 2013, Shi *et al.* 2022a, Shi *et al.* 2022b, Shi *et al.* 2023). These studies are instructive for understanding the mechanism of tunnel-embankment interaction.

Since embankments are usually subjected to cyclic loads such as vehicles, seepage, tidal action (Li *et al.* 2021), etc., the settlement of river embankments when tunnels pass may be much larger than the settlement of the greenfield ground surface (Liang *et al.* 2020). Based on a case study, Yan (2020) carried out three-dimensional numerical parametric studies to investigate the influence of the compression modulus of the fill, grouting level and the stress release ratio of the surrounding rock on the river embankment settlement subjected to tunnel undercrossing.

The study found that the maximum surface settlement decreases with the increase of the modulus of both the fill and grouting layer. The maximum surface settlement slightly decreases with the decrease of the stress release ratio of the surrounding rock. Lin *et al.* (2013) reported a case study of slurry shield under-passing embankments in Hangzhou. They identified the main factors affecting embankment settlement and proposed key technologies and construction control measures for settlement control during the slurry shield excavation. According to Zhou *et al.* (2021), the authors reported the key technologies in the construction process of the large-size slurry shield tunnel during its crossing of the Yangtze River Delta. The core difficulties are the control of slurry pressure and the poor structural stiffness of the embankment. A series of countermeasures are provided to ensure the safety of embankment and shield tunnel.

Lin *et al.* (2020) developed an analytical method to estimate the embankment's settlement and horizontal strains due to tunnelling with considering the embankment's self-weight, the property of the soil-embankment interface, and the embankment's stiffness. Subsequently, they proposed a procedure to evaluate the embankment's damage level based on the calculated tensile strain. It is found that embankment's bending stiffness plays more important role in the embankment's response compared with self-weight. Jiang and Yu (2014) conducted three-dimensional finite element method base on the background of a large diameter slurry shield obliquely under-passing embankment of the Yangtze River. The settlement of the embankment is analyzed under different cross angles and tunnel depths.

As far as author is aware, in most of the cases where the tunnel intersects with the river embankment, the tunnel and embankment are either perpendicular or intersect with large angle. Previous studies have not considered the extreme working condition of tunnels parallel to river embankments, nor have they conducted in-depth studies on the control factors which affect the tunnel-embankment interaction. To address those issues mentioned above, this paper presents a case study of two EPB shield tunnels that run parallel to a river embankment. The filed monitoring result was reported and discussed. A three-dimensional numerical back-analysis was then carried out to calibrate numerical model parameters and further interpret the ground movement

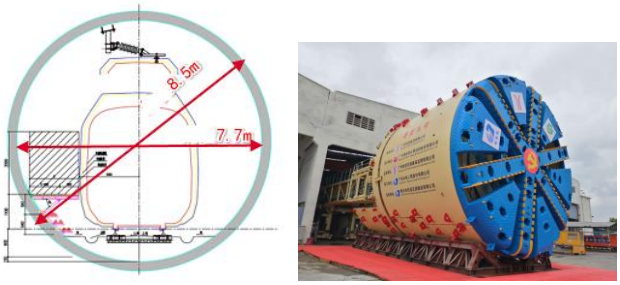

Fig. 1 Shield tunnel cross-section dimensions and shield machine photos of ChenXi section

contour. The prediction for ultimate embankment settlement was given. Afterwards, numerical parametrical study was conducted to explore the effect of tunnel face pressure, tail grouting pressure and volume loss on riverbank settlement. The necessity of reinforcing the river embankment and the optimal reinforcement depth have also been demonstrated. Finally, conclusions were drawn and suggestions for the design and construction of shield tunnel were given.

2. Engineering overview

Guangzhou Metro Line 22 is the first high-speed urban rail line in China with a design speed of 160 km per hour.

The total length of this line is 30.5 km, all the stations are underground. Among them, ChenTouGang Station - XiSan Station section (short for ChenXi section) is constructed with shield tunnel, consist of left line tunnel and right line tunnel. The total length of ChenXi section is 2748 m. The outer diameter and inner diameter of tunnel segments are 8.5 m and 7.7 m, respectively. The shield machine adopts earth pressure balance system with cutter plate diameter of 8.82 m. Fig. 1 shows the cross-section dimension of tunnel segment lining and the shield machine photo.

The general layout of Chenxi section is plotted in Figure 2a. Restricted by the location of the adjacent stations, and to avoid underpassing the pile foundations of highway bridges, the ChenXi section is designed to parallel to ShenChong River at mileage 54+520~54+900. The parallel length is about 380 m. Within the above mileage, the left line tunnel is mainly located below the riverbed with a burial depth of about 25-29 m. While the right line tunnel is located below the river east coast embankment with a burial depth of about 31-35 m.

The east coast embankment of the ShenChong River was built in 2008. The top of the embankment is a municipal road with a width of 8 m. The waterward side of the embankment is a concrete retaining wall, and the foot of the slope is backfilled with rocks. The strata underlying the embankment are (from top to bottom) plain fill, sludgy sand, sludge, silty clay, strongly weathered clastic rock, moderate weathered clastic rock and slightly weathered clastic rock, which is shown in Fig. 2(b). The shield tunnel mainly passes through the moderate weathered clastic rock layer and slightly weathered clastic rock layer. The typical

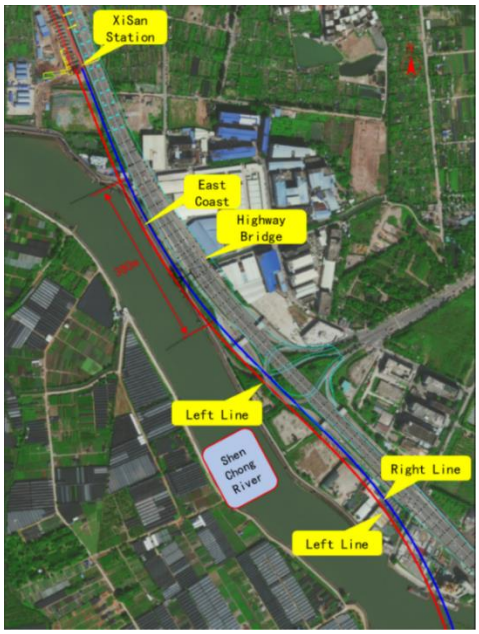

(a)

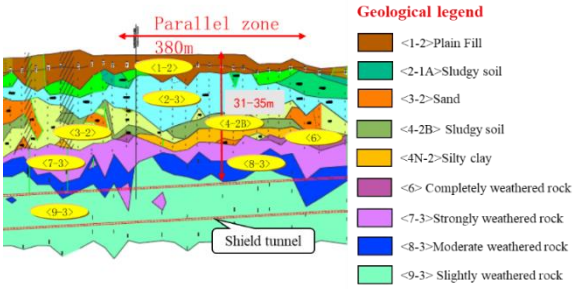

(b)

Fig. 2 (a) General layout of ChenXi section and (b) Geological profile of tunnel in parallel zone

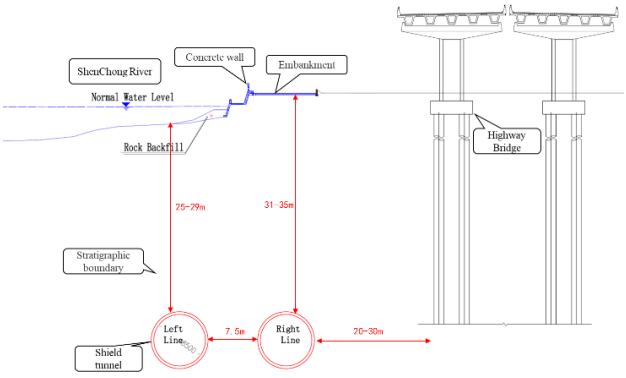

Fig. 3 Typical cross-sectional view of the tunnel undercrossing the river embankment

cross-sectional view of the tunnel undercrossing the river embankment is shown in Fig. 3.

Currently, the right line tunnel has successfully passed through the embankment parallel zone. The monitoring data of embankment deformation and tunnel lining is within allowable limits, which will be reported and discussed later. The left line has not yet started to cross the embankment parallel zone.

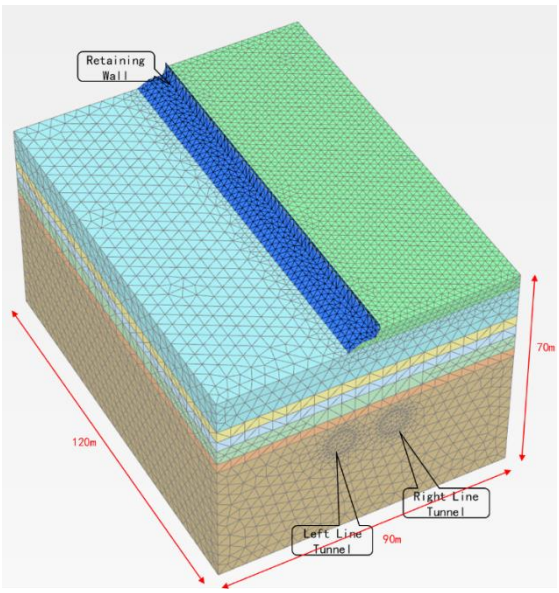

Fig. 4 Three-dimensional finite element mesh for numerical model

3. Numerical modeling

In this study, a series of three-dimensional numerical analysis was performed using the finite element program Plaxis 3D. A numerical back-analysis was first conducted based on the real case condition mentioned earlier. The reliability of numerical model adopted in this study were examined with the field monitoring data. Subsequently, the final deformation of the embankment was predicted. Parametric study on the tunnel-embankment interaction was conducted by varying the tunnel face pressure and tail grouting pressure.

3.1 Finite element mesh and boundary conditions

The model geometries and tunnel positions in the finite element mesh were identical to realistic engineering and stratigraphic condition. To minimize the boundary effect, the length (along the tunnel), width, depth of numerical model are 120 m, 90 m and 70 m, respectively. The distance from the tunnel to the bottom and side boundary of the model are 30 m and 32 m, which are over 3.5 times the tunnel diameter, respectively. Roller support and pin support were applied to the vertical and horizontal boundaries of the mesh, respectively. The bridge was not simulated since the bridge is far from the tunnel, and the focus of this study is the response of the river embankment.

Fig. 4 shows the finite element meshes adopted in this study. The thickness of the shield shell and segment lining are 60mm and 400 mm, respectively. An element type of 10-node tetrahedral is adopted to model the solid element (i.e., soil, segment lining). The shield shell was modelled using plate elements. The model consists of a total of 158247 elements and 223260 nodes. Parameter studies on the mesh density and model size have been conducted to ensure the accuracy of model. The phreatic surface was set at normal water level referred to Fig. 3. The stress-seepage

Table 1 Model parameters of soil layers

Stratum	ρ g/cm^3	C kPa	φ	ν	m	$E_{50}^{ref}/E_{oed}^{ref}$ MPa	E_{ur}^{ref} MPa	G_0^{ref} MPa
Plain fill	1.86	18	15	0.41	0.5	4	23	69
Sludgy Sand	1.85	1	28	0.32	0.5	8	39	117
Sludge	1.74	12	8	0.43	0.5	2	15	45
Silty clay	19.8	18	12	0.33	0.5	5	27	81
Strongly weathered clastic rock	2.55	38	27	0.31	0.5	16	71	213
Moderate weathered clastic rock	2.56	80	28	0.32	0.5	600	1800	-
Slightly weathered clastic rock	2.6	150	35	0.23	0.5	1000	3000	-
Cement reinforced soil	2.0	60	25	0.3	0.5	25	100	300

coupling effect was not considered since the permeability coefficient of the rock layer is low.

3.2 Constitutive model and model parameters

The key issue of finite element analysis is a suitable constitutive model of soils. However, all constitutive models were built based on several hypothesis and only reflects part of the soil characteristics. Therefore, all constitutive models have its limitations. After considering the regional characteristics of the soil and the overview of this project. The constitutive model of hardening soil model with small strain stiffness (HSS) is adopted in this study to model the soil layers. The HSS model describes the nonlinear stress-strain behaviour of soils under various loading conditions. This model considers the effects of soil structure, initial stress state, stress path, strain rate, and strain history on the soil response. This model also incorporates the concept of small strain stiffness, which means that the soil stiffness is much higher at very low strains than at higher strains. This model is an isotropic hardening elastoplastic model, which is suitable for the description of failure and deformation behaviour of many soil types. The HSS model can also distinguish the difference between loading and unloading, which means it is suitable for simulating excavation condition, as demonstrated in this study. The moderate weathered clastic rock and slightly weathered clastic rock are simulated using the hardening soil (HS) model.

After extensive trial calculations, the parameter values of the constitutive model are calibrated and verified based on field monitoring data. The values of model parameters for soil and rock layers are summarized in Table 1. Those parameters are basically based on the geotechnical investigation report of this project.

The concrete and steel were modelled as a linear elastic material. Table 2 shows the model parameters for the concrete and steel.

Table 2 Model parameters of elastic material

	ρ g/cm^3	E GPa	ν
Segment (concrete)	2.5	34.5	0.2
Shield shell (steel)	7.85	200	0.3

3.3 Numerical modelling steps

The modeling procedures are designed as follows:

1.Established the initial boundary and stress conditions of soil. The river embankment and its retaining wall were also modeled.

2. The right line tunnel is excavated first. Deactivate the soil inside the first and second excavation step, activate the shield shell and apply pressure on the tunnel face. The length of each excavation step is 5m. Apply surface contraction on the shield shell for simulating volume loss.

3. Deactivate the soil inside the third excavation step, activate the tunnel segment and grouting pressure.

4. Move the shield shell, tunnel face and segment lining forward.

5. Repeat step 4 until excavation of right line tunnel were finished.

6. Repeat the identical excavation procedure for left line tunnel.

4. Interpretation of field monitoring data

To achieve information-based construction and timely feedback during construction, as well as timely supplementary grouting when deformation exceeds the limit, a systematic monitoring network is established before tunnel underpass the embankment. In total, 89 ground settlement monitoring points were arranged on the surface of the embankment at a spacing of 10m, which is shown in Fig. 5.

The right line tunnel started to underpass the embankment at March 9, 2022 and completed passing through at April 29. The measured embankment settlement along the longitudinal direction of tunnel was plotted in Fig. 6. The data at two time points, when the tunnel had just completed passing through and five months after passing through, were plotted for comparison.

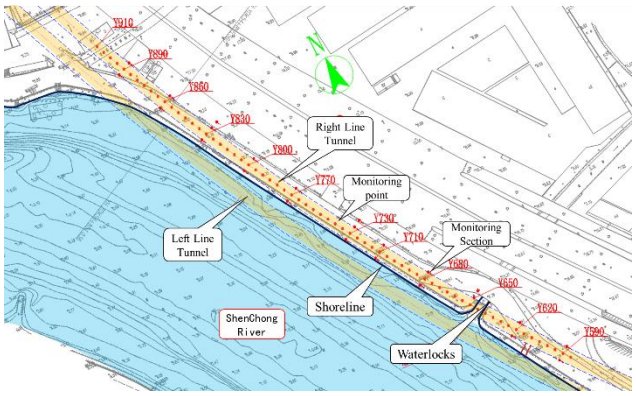

Fig. 5 Settlement monitoring points layout

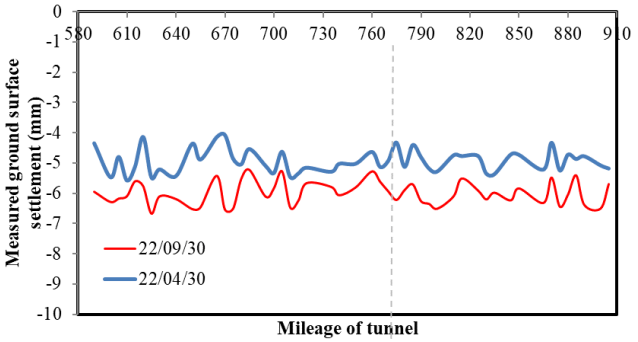

Fig. 6 Measured embankment settlement along the longitudinal direction of right line tunnel

When the tunnel had just completed passing through, the surface settlement ranged from 3.32 mm to 6.2 mm, with an average settlement of 4.88 mm. The maximum settlement occurred at mileage of 54+610. The settlement curve is not smooth, and the reasons for the fluctuations of data may be as follows: Firstly, the top of the river embankment is a municipal road, and the monitoring point is set on the road surface. Certain errors occurred when the monitoring point is subject to repeated impact from the traffic. Secondly, the embankment itself may settle under cyclic loads such as vehicle loads and seepage pressure due to tidal effect. Thirdly, the stratum is not uniformly distributed, the thickness of the soft soil layer and the rock layer above the tunnel could determine the surface settlement. Fourthly, the discontinuity of shield construction control - changes in face pressure, tail grouting pressure and operations (i.e., shield shutdown, shield opening and tool replacement) will result in fluctuations in the data.

About five months after the shield tunnel underpass, the monitoring data tends to be stable. The measured settlement slightly increased, the final data ranged from 4.53 mm to 7.43 mm. The maximum settlement occurred at mileage of 54+625, probably due the large thickness of soft soil layer at this location.

Apart from the deformation monitoring, crack observations have also been conducted on pavement and retaining wall of the river embankment. A total of 436 obvious cracks were observed before the tunnel excavation. After the tunnel underpass, no obvious change was observed at the original cracks, and no new crack occurred.

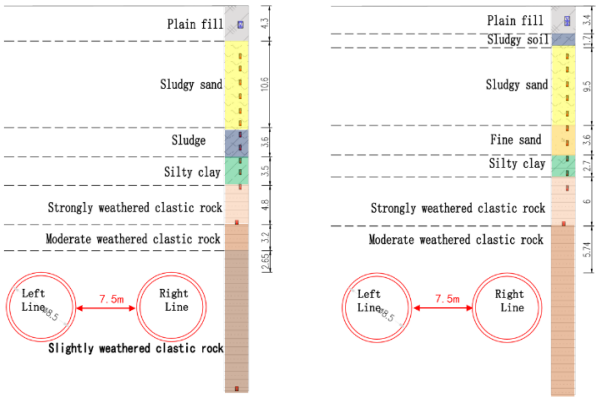

borehole 1 borehole 2

Fig. 7 Stratigraphic columns of borehole 1 and borehole 2

In addition, physical exploration methods such as radar scanning were also conducted on the river embankment to detect the potential cavity beneath the roadbed. The detection results showed that the roadbed foundation is relatively stable and there are no obvious voids or cavities. The above monitoring results and geophysical prospecting results jointly confirm a fact: for the given in this study, the tunnel excavation has small impact on the embankment.

5. Back-analysis and prediction

In fact, the boundary of the stratum is undulating and not uniformly distributed. Therefore, two back-analysis numerical models were established based on the stratigraphic columns of two typical boreholes. The stratigraphic columns of borehole 1 and borehole 2 are shown in Fig. 7. Borehole 1 and borehole 2 represent the best and worst geological conditions within the region where the tunnel is paralleled to the river embankment. The tunnel was excavated in slightly weathered clastic rock and moderate weathered clastic rock, respectively. The default tunnel face pressure and tail grouting pressure are 550 kPa and 300 kPa, according to the construction record. The volume loss of shield tunnel is set to 0.75%.

Figs. 8(a) and 8(b) compares the computed embankment surface settlement contour of two numerical models after the right line tunnel passed through. The model B1 and B2 represent the numerical model corresponding to borehole 1 and borehole 2, respectively. The commonality between the two model results is that the maximum settlement occurred at the middle of model, above the right line tunnel. This is because the river embankment in the middle of the model has undergone the entire process of shield tunnel crossing, while those elements near the boundary did not. The maximum ground surface settlement in model B1 is 3.47 mm, which is about 40% of that in model B2 (8.57 mm).

This is because the soil around the tunnel in model B1 is slightly weathered clastic rock, which has higher stiffness and strength than moderate weathered clastic rock. Therefore, the surrounding soil's disturbance and surface deformation caused by new tunnel excavation are much smaller. On the other hand, due to the non-uniformity of the

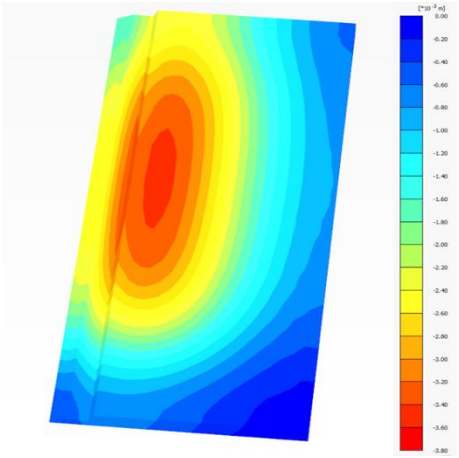

(a) Model B1

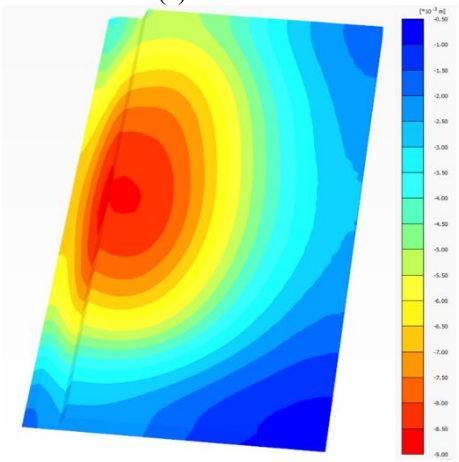

(b) Model B2

Fig. 8 Computed embankment settlement contour after right line tunnel was excavated

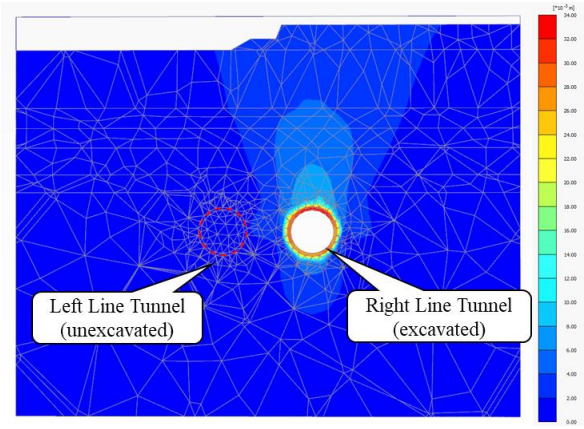

(a) Model B1

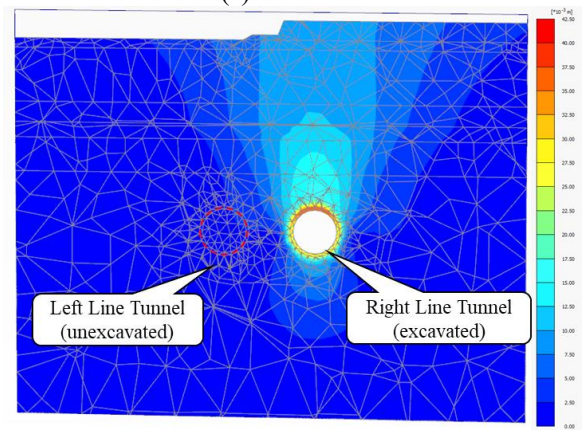

(b) Model B2

Fig. 9 Computed soil displacement contour after right line tunnel was excavated

strata, the computed surface settlement of models B1 and B2 correspond respectively to the lower limit and upper limit of the settlement under realistic strata distribution condition. That is to say, the real settlement should be between the lower limit (3.47 mm) and the upper limit (8.57 mm). This is also basically consistent with measured data (range from 4.53 mm to 7.43 mm), which proves that the finite element method, constitutive model and simulating procedure adopted in this study is credible.

Other finding is that the settlement trough of model B1 seems to be narrower than that in model B2. The sectional settlement contour may help to better understand this phenomenon, which are plotted in Figs. 9(a) and 9(b). The selected section is located where the maximum settlement occurs. In both models, the displacement of the soil mainly occur around the tunnel due to volume loss caused by tunnel excavation. The maximum soil displacement in model B1 and B2 are 33.4 mm and 37.9 mm, respectively.

The ratio of maximum embankment settlement to maximum displacement of soil is 10% and 23%, respectively. Moreover, the expansion angle of settlement trough in model B2 (about 45 degree) is larger than that in model B1 (about 30 degree). Due to the high strength (i.e., cohesion) of slightly weathered clastic rocks, relatively small arch height is mobilized to generate the soil-arching effect. The stress release caused by tunnel excavation is mainly sustained by the slightly weathered rock layer. Therefore, the disturbance to the ground surface subjected to tunnel excavation in slightly weathered clastic rock is negligible, even if there is soft soil in this area. However, this phenomenon is relatively insignificant when the tunnel is buried in moderate weathered clastic rock

Fig. 10 plots the computed maximum embankment settlement at each excavation step. The commonality of two curves is that most of the settlement occurs when the distance between tunnel face and monitoring section is within the range of -3D to +3D, where D represents the diameter of the tunnel excavation. In other word, when the distance between the tunnel face and the monitoring section exceeds 3D, the influence of tunnel excavation on the embankment settlement is relatively low. When the excavation of the left line tunnel was completed, the maximum surface settlement of models B1 and B2 were 5.65 mm and 17.54 mm respectively, which increased by 63% and 105% compared to when the right line excavation was completed. In model B1, the embankment settlement induced by the left line tunnel is lower than that of the right line tunnel. The reason is that the right tunnel is laid directly below the embankment, while the left tunnel is farther away from the embankment in space. However, the embankment

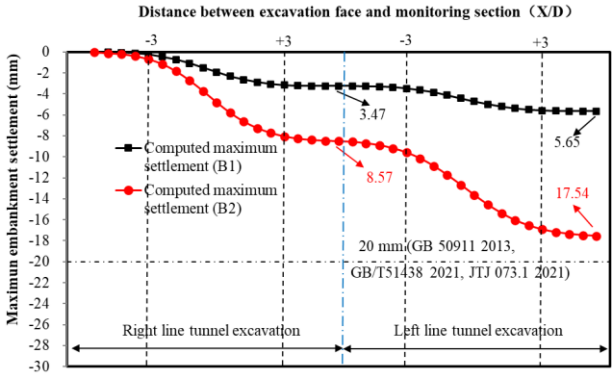

Fig. 10 Computed embankment settlement at each excavation step

settlement caused by the left line tunnel is slightly higher than that from the right line tunnel in model B2. One possible reason is that larger plastic zone of soil was mobilized in model B2, which has been previously discussed. After the right tunnel was excavated, the soil under the embankment had already partially entered the plastic stage, and their stiffness decreased. Consequently, when the left tunnel was excavated, larger plastic deformation would be generated inside the embankment.

According to the numerical back-analysis results, the ratio between ultimate maximum embankment settlement and the maximum embankment settlement due to right line tunnel is 163%~205%. The higher the weathering degree of surrounding rock, the greater the ratio. By enlarging the on-site monitoring embankment settlement (vary from 4.53 mm to 7.43 mm) with the same ratio, the ultimate embankment settlement is estimated to be between 7.38 mm and 15.23 mm. Even so, the predicted maximum embankment settlement is still within the allowable limit (20 mm) of the associated codes (GB 50911 2013, GB 50286 2013, GB/T51438 2021, JTJ 073.1 2021). This once again confirms that the tunnel excavation underneath the riverbank in this case will hardly affect the safety and serviceability of the embankment.

6. Effect of tunnel face pressure, tail grouting pressure and volume loss on river embankment settlement

The numerical parametrical studies conducted in this study were summarized in Table 3.

To obtain a comprehensive understanding of shield tunnel induced embankment settlement, three series of parametric studies considering different tunnel face pressures, tail grouting pressures and volume losses were conducted. To study the sensitivity of tunnel face pressure (P_f) on embankment settlement, 5 values of P_f were considered (i.e., 100, 200, 300, 400 and 500). The 300 kPa is approximately equal to $K_0\sigma_v$. The K_0 and σ_v represent the coefficient of earth pressure at rest and original vertical soil pressure at the centerline of the tunnel, respectively. To investigate the influence of tail grouting pressure (P_g) on multiple tunnel interaction, 5 values of P_g were considered

Table 3 Parametric studies performed in this study

Series	Tunnel face pressure P_f (kPa)	Tail grouting pressure P_g (kPa)	Volume loss (%)
2	100 200 **300** 400 500	550	0.75
1	300	350 450 550 650 750	0.75
3	300	550	0.25 0.5 0.75 1.0 1.25

in this study (i.e., 350, 450, 550, 650 and 750 kPa). The 750 kPa is approximately equal to σ_v. In addition, 5 values of new tunnel excavation induced volume loss were considered (i.e., 0.25%, 0.5%, 0.75%, 1.25% and 1.5%).

The high-volume loss represents the condition with poor management and control of tunnel construction. Both model B1 and model B2 participated in the parametrical studies. It is worth mentioning that according to the construction records during the process of crossing the river embankment, the tunnel face pressure is between 0.25 and 0.4 MPa, and the tail grouting pressure is between 0.3 and 0.6 MPa.

Fig. 11(a) shows the maximum embankment settlement considering different tunnel face pressures (P_f). As expected, the settlement of the embankment is negatively correlated with the P_f. When the P_f increased from 100 kPa to 300 kPa, the maximum embankment settlement in models B1 and B2 decreased from 6.56 mm and 21.58 mm to 5.65 mm and 17.54 mm, respectively, decrease by 13.9% and 18.7%. However, when the P_f increased from 300kPa to 500 kPa, the maximum settlement of models B1 and B2 decreased to 5.41 mm and 16.88 mm, respectively, whose relative reduction ratio are only 4.2% and 3.8%. Thus, it is optimal to control the P_f at 300 kPa. Further increasing the P_f does not help control the embankment settlement lot. It is worth mentioning that when p_f is equal to 100 kPa, the maximum embankment settlement of model B2 exceeds the allowable limit (20 mm).

Fig. 11(b) shows the embankment settlement under different tail grouting pressures (P_g). The relationship between embankment settlement and P_g is similar to that of tunnel face pressure. As P_g increases, the embankment settlement tends to decrease. When the P_g rises from 350 kPa to 750 kPa, the maximum embankment settlement in model B1 decreases from 6.56 mm to 4.88 mm, the reduction ratio is up to 25.6%. Under the same grouting pressure change, the maximum embankment settlement in

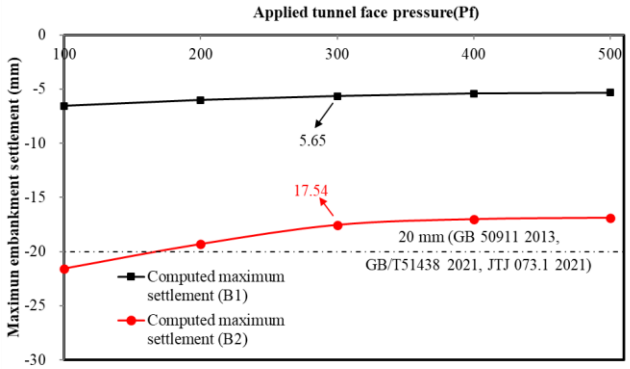

(a) Tunnel face pressure (kPa)

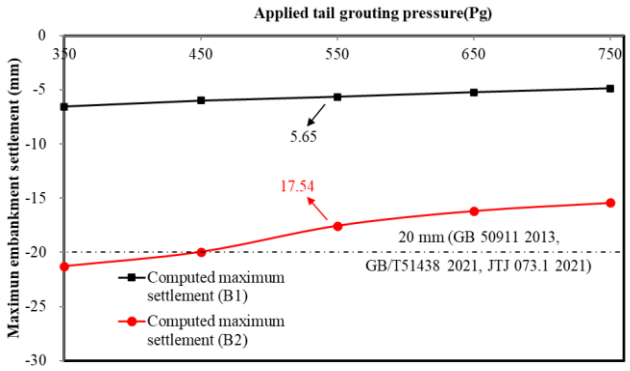

(b) Tail grouting pressure (kPa)

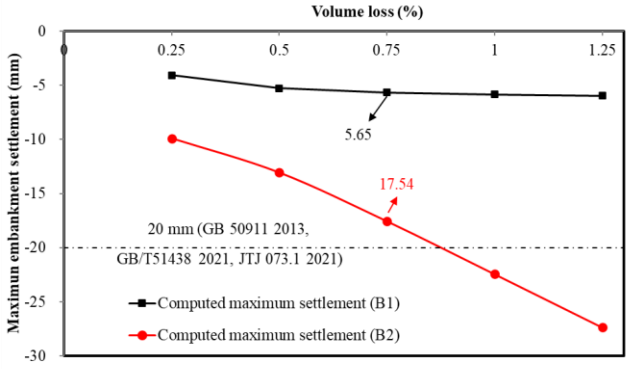

(c) Volume loss (%)

Fig. 11 The maximum embankment settlement with the variety of:

model B2 decreases from 21.29 mm to 15.43 mm, the reduction ratio is up to 27.5%. Similarly, when the P_g is too low (i.e., 350 kPa), the embankment settlement in model B2 also exceeds the allowable limit. With the increase of grouting pressure, there is no obvious attenuation of the rate of decrease of embankment settlement. However, excessive grouting pressure is not recommended because it will cause excessive stress on the tunnel segment lining and break through the sealing pads.

Fig. 11(c) illustrates relationship between maximum embankment settlements with volume losses induced by new tunnel excavation. In this study, volume loss varied from 0.25% to 1.25%. For both models, the embankment settlement increased with the increase of volume loss. At

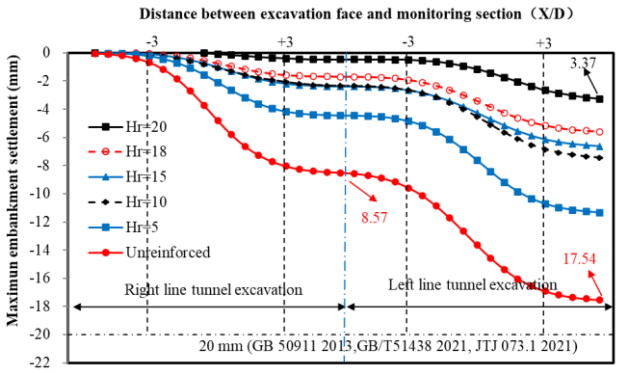

Fig. 12 Effect of reinforcement depth on the tunnelling induced embankment settlement

volume loss of 0.25%, the maximum embankment settlements are 4.05 mm and 9.89 mm, respectively. When the volume loss increases to 1.25%, these two values rise to 5.97 mm and 27.33 mm. The embankment settlement under the maximum volume loss condition is 1.47 times and 2.76 times that under the minimum volume loss condition, respectively. Is clear that the embankment settlement is significantly sensitive to volume loss in model B2. Perhaps due to the self-stability of slightly weathered rock layer. Even under the condition of poor tunnel construction control, most of the tunneling induced soil disturbance can be controlled within the rock layer. However, when tunnels are excavated in moderate weathered rock layer, good workmanship is quite necessary. According to the computed results, embankment settlement will exceed the allowable limit if volume loss exceeds 1%.

Although the settlement of the river embankment is to some extent affected by tunnel face pressure and tail grouting pressure, their impact on the river embankment is far less than that from volume loss. Therefore, apart from determining reasonable face pressure and the tail grouting pressure, strengthening the construction control of shield tunnel for reducing volume is much more important.

According to the above results, when the tunnel is excavated in moderate weathered rock layer, it is possible for the embankment settlement to exceed the allowable limit if the control of face pressure, tail grouting pressure and volume loss is inappropriate. Alternatively, when tunnels are buried in soft soil, the response of river embankment would significantly increase. Therefore, it is meaningful to discuss the necessity and effectiveness of reinforcing the river embankment in advance.

The reinforcement method to be selected for the river embankment is cement mixing pile, and the reinforcement scope is the entire width range of the embankment. Due to the difficulty of operation on water, the reinforcement of the soft soil within the riverbed range is not considered. It is meaningless to reinforce the embankment when tunnel is excavated in slightly weathered rock. This chapter is based on model B2 and studies the disturbance of the river embankment by tunnel excavation under various reinforcement depth (H_r) conditions. In total, 5 reinforcement depth (i.e., 20 m, 18 m, 15 m, 10 m and 5 m) were considered. Refer to Fig. 7, the Hr =20, 18, 15

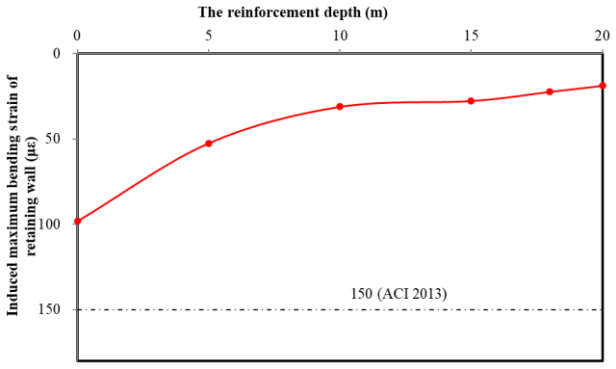

Fig. 13 Relationship between reinforcement depth and bending strain of retaining wall

respectively represent that the cement mixing pile reached the bottom of the silty clay layer, fine sand layer and sludgy sand layer. The Hr = 10 and 5 represent the conditions when the bottom of pile is located in the middle of the sludgy sand layer or at the bottom of the sludgy soil layer.

The cement reinforced soil is simulated with HSS model, whose model parameters are listed in Table 1.

Fig. 12 compares the maximum river embankment settlement under several reinforcement depth conditions (including the unreinforced case). When the reinforcement depth is 20 m, the excavation of the right line tunnel only caused embankment settle 0.47 mm. The ultimate settlement was only 3.37 mm, which was 80% less than the unreinforced case. When the reinforcement depth is 18 m, 15 m, and 10 m, the ultimate embankment settlement are 5.6 mm, 6.63 mm and 7.44 mm, respectively, which are 68%, 62% and 58% lower than the unreinforced case. Even when the reinforcement depth is only 5 m, the river embankment is 35% lower than the initial condition, at 11.33 mm. From the perspective of the ratio of the reduction of river embankment settlement to the reinforcement depth, the cost-effectiveness of reinforcement depth of 5 m or 10 m is the highest. In fact, the reinforcement depth should be determined according to the allowable value of settlement.

Another finding is that larger proportion of the embankment settlement took place during the excavation of left line tunnel. And this phenomenon became more obvious as the reinforcement depth increased. This is because the reinforced soil is located directly above the right line tunnel, and the increase in strength and stiffness has more restriction effect on the soil disturbance due to right line tunnel excavation.

Fig. 13 shows the variation of the retaining wall's bending strain with reinforcement depth induced by new tunnel excavation. The bending strain is equal to M/WE, where M, W and E represent the bending moment, section modulus and young's modulus of the retaining wall. For the case where river embankment is unreinforced, the incremental bending strain of the retaining wall caused by shield tunnel is 98.1με, about two-thirds of the allowable tensile strain of unreinforced concrete of 150 με (ACI 2001). This also matches the on-site result that no new crack or development of original crack was observed. This confirms the point that the impact of tunnel excavation on the embankment structures is minimal with given geometry and stratigraphic condition in this study. When the reinforcement depth is increased to 5m, the bending strain of the retaining wall decreases to 52.4με. On the one hand, this is due to the decrease in embankment settlement, and on the other hand, it is due to the increase in soil stiffness, which has a greater restriction on retaining wall's bending deformation. When the reinforcement depth increased to 10m, the bending strain of the retaining wall decreases to 37.64με. However, this trend is not linear. When the reinforcement depth is increased to 15m, 18m and 20m, the bending strain of the retaining wall is 23.54, 21.3 and 19.74 respectively. Compared with the case where the reinforcement depth is 10mm, the decrease ratios are 15%, 23% and 28%. This means that after the reinforcement depth exceeds 10m, continuously increasing reinforcement depth is inefficient for the protection of the river embankment structure. The reinforcement depth is already large enough. Although tunnel excavation can cause overall consolidation settlement of the unreinforced soil, it will not generate excessive uneven settlement and internal forces in embankment structure.

7. Conclusions

This study provides a valuable case of two EPB shield tunnels parallelly undercrossing a river embankment. With interpretation of on-site monitoring data, three-dimensional numerical back-analysis and parametrical analysis, the mechanism of the impact of tunnel excavation on river embankments was discussed. Furthermore, key countermeasures for protecting the embankment are suggested based on the parametrical studies.

(1) According to the field monitoring data, the settlement of the embankment after the excavation of the right line tunnel is 4.53 mm ~ 7.43 mm. Neither new crack on the pavement or cavity under the roadbed was observed.

(2) It is found that the higher the weathering degree of the tunnel surrounding soil, the greater the embankment settlement and the wider the settlement trough. This is because the soil-arching effect require higher arch height if the soil strength is lower, and the range of plastic zone is larger. This also leads to decrease in the stiffness of the soil mass under the embankment after the excavation of the first tunnel. Thus, the latter excavated tunnel might cause larger deformation.

(3) For the given condition in this study, where the tunnels are buried in moderate weathered clastic rock and slightly weathered clastic rock, new tunnel excavation would hardly affect the safety and serviceability of the river embankment. The ultimate settlement of the embankment after the twin-tunnel excavation is predicted to be between 7.38 mm and 15.23 mm, which is within the allowable limit.

(4) The embankment settlement is negatively correlated with tunnel face pressure and tail grouting pressure with limited sensitivity. In this case, the recommended tunnel face pressure and tail grouting pressure are 300 kPa and 550

kPa, respectively. It is found that the factor which affect the embankment settlement most is volume loss. Special attention should be paid to control and compensate the volume loss caused by tunnel excavation.

(5) The pre-reinforcement has significant effect on reducing the tunnelling induced settlement and structure response of the embankment. When the thickness of overlying soft soil is large (this sort of soil layer is often found near the river embankment) or the river embankment has relatively high requirement for settlement control, reinforcing the soft soil below the river embankment in advance can help ensure the safe passage of the tunnel. The recommended reinforcement depth is 10 m, in case the predicted response of river embankment exceeds the allowable limit.

Acknowledgments

The research described in this paper was financially supported by Guangzhou Metro Design and Research Institute Co., Ltd (Research project number KY-2023-029).

References

ACI 224R-01 (2001), Control of cracking in concrete structures, American Concrete Institute; Farmington Hills, MI, USA.

Bai, X.D., Cheng, WC. and Li, G. (2021), "A comparative study of different machine learning algorithms in predicting EPB shield behaviour: a case study at the Xi'an metro, China", *Acta Geotechnica*, **16**, 4061-4080. https://doi.org/10.1007/s11440-021-01383-7.

Boonyarak, T. and Ng, C.W. (2014), "Effects of construction sequence and cover depth on crossing-tunnel interaction", *Can. Geotech. J.*, **52**(999), 1-17. https://doi.org/10.1139/cgj-2014-0235.

Chapman, D.N., Ahn, S.K. and Hunt, D.V.L. (2007), "Investigating ground movements caused by the construction of multiple tunnels in soft ground using laboratory model tests", *Can. Geotech. J.*, **44**(6), 631-643. https://doi.org/10.1139/t07-018.

Chen, L.A., Pei, W.W., Yang, Y.H. and Guo, W.L. (2022), "Three-dimensional numerical parametric study of shape effects on multiple tunnel interactions", *Geomech. Eng.*, **31**(3), 237-248. https://doi.org/10.12989/gae.2022.31.3.237.

Chi, S.Y., Chern, J.C. and Lin, C.C. (2001), "Optimized back-analysis for tunneling-induced ground movement using equivalent ground loss model", *Tunn. Undergr. Sp. Tech.*, **16**(3), 159-165. https://doi.org/10.1016/S0886-7798(01)00048-7.

Cui, C.Y., Zhang, S.P., Yang, G. and Li, X.F. (2016), "Vertical vibration of a floating pile in a saturated viscoelastic soil layer overlaying bedrock", *J. Southeast Univ.*, **23**(1), 220-232. https://doi.org/ 10.1007/s11771-016-3065-5.

Cui, C.Y., Zhang, S.P., Chapman, D. and Meng, K. (2018a), "Dynamic impedance of a floating pile embedded in poro-visco-elastic soils subjected to vertical harmonic loads", *Geomech. Eng.*, **15**(2), 793-803. https://doi.org/10.12989/gae.2018.15.2.793.

Cui, C.Y., Meng, K., Wu, Y.J., Chapman, D. and Liang, Z.M. (2018b), "Dynamic response of pipe pile embedded in layered visco-elastic media with radial inhomogeneity under vertical excitation", *Geomech. Eng.*, **16**(6), 609-618. https://doi.org/10.12989/gae.2018.16.6.609.

Cui, C.Y., Meng, K., Xu, C.S., Wang, B.L. and Xin, Y (2022) "Vertical vibration of a floating pile considering the incomplete bonding effect of the pile-soil interface", *Comput. Geotech.*, **150**, 104894. https://doi-org/10.1016/j.compgeo.2022.104894.

GB 50286 (2013), Code for design of levee project, Ministry of Water Resources of the People's Republic of China; Beijing, China.

GB 50911 (2013), Code for monitoring measurement of urban rail transit engineering, Ministry of Housing and Urban-Rural Development; Beijing, China.

GB/T51438 (2021), Standard for design of shield tunnel engineering, Ministry of Housing and Urban-Rural Development; Beijing, China.

Jiang, B., Chen, L., Yang, J.S., Wang, S.Y. and Ng, C.W.W. (2017), "Effects of twin-tunnel excavation on an existing horseshoe-shaped tunnel considering the influence of a settlement joint", *Can. Geotech. J.*, 54. https://doi.org/10.1139/cgj-2015-0389.

Jiang, Z.Y. and Yu, J. (2014), "The analysis of stratum settlement for a large diameter slurry shield obliquely under-passing embankment of the Yangtze River", *Adv. Mater. Res.*, **919**, 895-901. https://doi.org/10.4028/www.scientific.net/AMR.919-921.895.

JTJ 073.1 (2021), Technical specifications of cement concrete pavement maintenance for highway, Ministry of Communications of the People's Republic of China; Beijing, China.

Li, G., Cheng, WC. and Bai, X.D. (2022), "Analytical modelling of segmental liner joints for close-proximity tunnelling in soft ground", *Tunn. Undergr. Sp. Tech.*, **125**, 104495. https://doi.org/10.1016/j.tust.2022.104495.

Li, P., Sun, X., Chen, J. and Shi, J. (2021), "Effects of new construction technology on performance of ultralong steel sheet pile cofferdams under tidal action", *Geomech. Eng.*, **27**(6), 561-571. https://doi.org/10.12989/gae.2021.27.6.561.

Liang, Y., Chen, X., Yang, J. and Huang, L. (2020), "Risk analysis and control measures for slurry shield tunneling diagonally under an urban river embankment", *Adv. Civil Eng.*, **2020**, 1-11. https://doi.org/10.1155/2020/8875800.

Lin, C.G., Huang, M.S., Nadim, F. and Liu, Z.Q. (2020), "Embankment responses to shield tunnelling considering soil-structure interaction: Case studies in Hangzhou soft ground", *Tunn. Undergr. Sp. Tech.*, **96**, 103230. https://doi.org/10.1016/j.tust.2019.103230.

Lin, C.G., Zhang, Z.M., Wu, S.M. and Yu, F. (2013), "Key techniques and important issues for slurry shield under-passing embankments: a case study of Hangzhou qiantang river tunnel", *Tunn. Undergr. Sp. Tech.*, **38**, 306-325. https://doi.org/10.1016/j.tust.2013.07.004.

Mair, R.J., Taylor, R.N. and Bracegirdle, A. (1993), "Subsurface settlement profiles above tunnels in clays", *Géotechnique*, **43**(2), 315-320. https://doi.org/10.1680/geot.1993.43.2.315.

Nawel, B. and Salah, M. (2015), "Numerical modeling of two parallel tunnels interaction using three-dimensional finite elements method", *Geomech. Eng.*, **9**(6), 775-791. https://doi.org/ 10.12989/gae.2015.9.6.775.

Neaupane, K.M. and Adhikari, N.R. (2006), "Prediction of tunneling-induced ground movement with the multi-layer perceptron", *Tunn. Undergr. Sp. Tech.*, **21**(2), 151-159. https://doi.org/10.1016/j.tust.2005.07.001.

New, B.M. and O'Reilly, M.P. (1991), "Tunneling induced ground movements: predicting their magnitudes and effects", *Proceedings of the 4th International Conference on Ground Movements and Structures*, Cardiff, July.

Ng, C.W., Boonyarak, T. and Mašín, D. (2013), "Three-dimensional centrifuge and numerical modeling of the interaction between perpendicularly crossing tunnels", *Can.*

Geotech. J., **50**(9), 935-946. https://doi-org/ 10.1139/cgj-2012-0445.

O'Reilly, M.P. and New, B.M. (1982), "Settlement above tunnels in the United Kingdom–their magnitude and prediction", *In Tunnelling'82*, *Proceedings of the 3rd International Symposium*, London, June.

Park, K.H. (2004). "Elastic solution for tunneling-induced ground movements in clays", *Int. J. Geomech.*, **4**(4), 310-318. https://doi.org/10.1061/(ASCE)1532-3641(2004)4:4(310).

Peck, R.B. (1969), "Deep excavation and tunneling in soft ground", *Proceedings of the 7th International Conference on Soil Mechanics and Foundation Engineering*, Mexico City, Augest.

Shi, J.W., Ng, C.W.W. and Chen, Y.H. (2015), "Three-dimensional numerical parametric study of the influence of basement excavation on existing tunnel", *Comput. Geotech.*, **63**, 146-158. https://doi.org/ 10.1016/j.compgeo.2014.09.002.

Shi, J.W., Fu, Z.Z. and Guo, W.L. (2019), "Investigation of geometric effects on three-dimensional tunnel deformation mechanisms due to basement excavation", *Comput. Geotech.*, **106**, 108-116. https://doi.org/10.1016/j.compgeo. 2018.10.019.

Shi, J.W., Ding C., Ng, C.W.W., Lu, H. and Chen L. (2020), "Effects of overconsolidation ratio on tunnel responses due to overlying basement excavation in clay", *Tunn. Undergr. Sp. Tech.*, **7**, 103247. https://doi.org/10.1016/j.tust.2019.103247.

Shi, J.W., Wei, J.Q., Ng, C.W.W., Lu, H. Ma, S.K., Shi, C. and Li, P. (2022a), "Effects of construction sequence of double basement excavations on an existing floating pile", *Tunn. Undergr. Sp. Tech.*, **119**, 104230. https://doi.org/10.1016/j.tust.2021.104230.

Shi, J.W., Chen Y.H., Lu, H., Ma, S.K. and Ng, C.W.W. (2022b), "Centrifuge modeling of the influence of joint stiffness on pipeline response to underneath tunnel excavation", *Can. Geotech. J.*, **59**(9), 1568-1586. https://doi.org/10.1139/cgj-2020-0360.

Shi, J.W., Wang, J.P., Chen Y.H., Shi, C., Lu, H., Ma, S.K. and Fan, Y.B. (2023), "Physical modeling of the influence of tunnel active face instability on existing pipelines", *Tunn. Undergr. Sp. Tech.*, **140**, 105281. https://doi.org/10.1016/j.tust.2023.105281.

Yan L.L. (2020), "Numerical analysis of ground settlement caused by shield tunnel passing through river embankment", *J. Hunan City Univ. (Natural Science)*, **29**(6), 4. https://doi.org/10.3969/j.issn.1672-7304.2020.06.0002.

Yoo, C. and Cui, S.S. (2020), "Effect of new tunnel construction on structural performance of existing tunnel lining", *Geomech. Eng.*, **22**(6), 497-507. https://doi.org/10.12989/gae.2020.22.6.497.

Zhou, S., Ye, G.L., Han, L. and Wang, J.H. (2021), "Key construction technologies for large river-crossing slurry shield tunnel: case study", *J. Aerosp. Eng.*, **34**(2), 04020118. https://doi.org/10.1061/(ASCE)AS.1943-5525.0001236.

GC